arXiv:1511.08112v1 [quant-ph] 25 Nov 2015

Non-reciprocal nonlinear optic induced transparency and frequency conversion on a chip

Xiang Guo,[1] Chang-Ling Zou,[1] Hojoong Jung,[1] and Hong X. Tang*[1]

[1] *Department of Electrical Engineering, Yale University, New Haven, Connecticut 06511, USA*

Developments in photonic chips have spurred photon based classical and quantum information processing, attributing to the high stability and scalability of integrated photonic devices [1, 2]. Optical nonlinearity [3] is indispensable in these complex photonic circuits, because it allows for classical and quantum light sources, all-optical switch, modulation, and non-reciprocity in ambient environments. It is commonly known that nonlinear interactions are often greatly enhanced in the microcavities [4]. However, the manifestations of coherent photon-photon interaction in a cavity, analogous to the electromagnetically induced transparency [5], have never been reported on an integrated platform. Here, we present an experimental demonstration of the coherent photon-photon interaction induced by second order optical nonlinearity ($\chi^{(2)}$) on an aluminum nitride photonic chip. The non-reciprocal nonlinear optic induced transparency is demonstrated as a result of the coherent interference between photons with different colors: ones in the visible wavelength band and ones in the telecom wavelength band. Furthermore, a wide-band frequency conversion with an almost unit internal (0.14 external) efficiency and a bandwidth up to 0.76 GHz is demonstrated.

The importance of integrating nonlinear devices on a photonic chip has become more prominent due to the devices' small foot-prints and large scalability [6, 7]. Second order optical nonlinearity ($\chi^{(2)}$) is one of the most widely explored properties in photonics, utilizing various nonlinear materials [8–13]. $\chi^{(2)}$ nonlinearity enables the coupling between photons with very different colors, acting as the basis for many important applications such as second harmonic generation, spontaneous parametric down conversion, optical parametric amplification and oscillation. Due to the high quality factor to mode volume ratio, the nonlinear interaction strength is expected to be boosted in optical cavities. Preliminary results in millimeter sized optical resonators have already shown such trend, where efficient second harmonic generation [14, 15] and sum frequency generation [16] are demonstrated. However, the realized nonlinear interaction strength on an integrated platform is normally weak, hindered by the challenges of fabricating small size, low loss optical circuits with materials featuring high $\chi^{(2)}$ nonlinearity.

In this Letter, we demonstrate coherent interaction between photons of different colors on a scalable aluminum nitride-on-insulator [12] chip based on $\chi^{(2)}$ optical nonlinearity. The nonlinear optic induced transparency (NOIT), as an analogue to electromagnetically induced transparency resulting from coherent photon-atom [5] or photon-phonon interactions [17–20], is reported. Due to the inherent phase matching condition, the $\chi^{(2)}$ nonlinearity based coherent interaction and the accompanying NOIT phenomenon are non-reciprocal [19, 20], which permits future applications such as non-magnetic, ultrafast optical isolators [21–23]. We further realize a saturated frequency conversion from telecom band to visible band with almost unit internal (0.14 external) conversion efficiency. Notably, the transparency window demonstrated here is close to GHz, which is orders of magnitudes larger than the bandwidth of previously demonstrated transparency [17–20] and wavelength conversion [24, 25] induced by opto-mechanical interaction. This large bandwidth, together with a flexible working environment (ambient air - no need for cryogenic cooling or vacuum system), may be beneficial for applications including optical switches, isolators and frequency converters.

Figure 1a illustrates the fabricated aluminum nitride (AlN) microring structure, which includes two bus waveguides that couple with the telecom and visible modes in the microring separately. The $\chi^{(2)}$ nonlinearity of the AlN induces the interaction between three non-degenerate modes, as described by the Hamiltonian

$$\mathcal{H} = \omega_{a0}\hat{a}^\dagger\hat{a} + \omega_{b0}\hat{b}^\dagger\hat{b} + \omega_{c0}\hat{c}^\dagger\hat{c} + g(\hat{a}\hat{b}^\dagger\hat{c} + \hat{a}^\dagger\hat{b}\hat{c}^\dagger). \quad (1)$$

Here, $\hat{a}$, $\hat{b}$ and $\hat{c}$ are the bosonic operators for three transverse-magnetic (TM) modes in the microring. In our experiment, we choose modes a, c in the telecom band and mode b in the visible band. On one hand, the momentum conservation condition ($m_a + m_c = m_b$) is required for a non-vanishing interaction strength g, which demands modes traveling in the same direction in the microring resonator. On the other hand, the nonlinear interaction in the microring can only be maximally enhanced when the energy conservation condition $\omega_{a0} + \omega_{c0} = \omega_{b0}$ is satisfied. We carefully engineer the device geometry and find the modes that satisfy both conservation conditions. The measured transmission spectra of the modes (with loaded quality factors $Q_{a,b,c} = (1.8, 1.0, 2.6) \times 10^5$) and the schematic diagram of their density of states in frequency domain are presented in Fig. 1b.

As we aim for the coherent conversion between the telecom and visible photons, we strongly drive mode a by a near resonance strong laser (ω_a) and hence stimulate

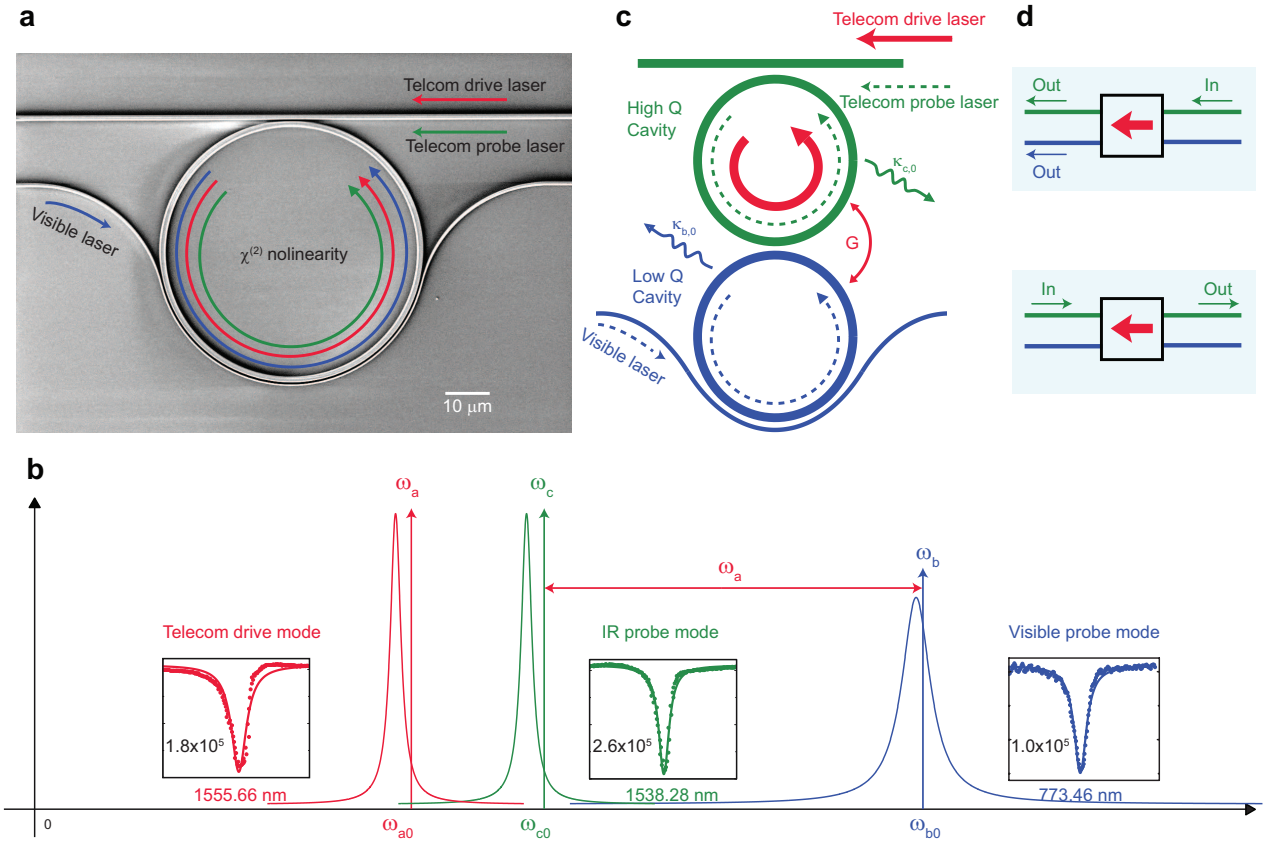

FIG. 1: **Triply resonant microring resonators coupled by second order optical nonlinearity. a**, SEM picture of the core device. Three transverse-magnetic modes (two in the telecom band, one in the visible band) co-exist in the microring resonator, and couple through $\chi^{(2)}$ nonlinear interaction. **b**, Schematic sketch of the density of states for the three modes and their respective transmission spectrum. At the triply resonant condition, the three modes' frequencies approximately fulfill the energy conservation requirement $\omega_{a0} + \omega_{c0} = \omega_{b0}$. **c**, Coupled resonator model for the coherent interaction in a $\chi^{(2)}$ microring resonator. Here we use two resonators to depict resonant modes supported at two different wavelengths. The interaction between them is through $\chi^{(2)}$ nonlinearity and the coupling strength is controlled by the power of the drive laser. **d**, A further simplified four-port block model to describe the nonlinear interaction. Here the device works as a two-in-two-out beamsplitter, whose splitting ratio is controlled by the power of the drive laser. The device is non-reciprocal due to the required momentum conservation condition in $\chi^{(2)}$ conversion process.

large exchange coupling strength between mode b and c. The simplified system Hamiltonian reads

$$\mathcal{H} = \omega_{b0}\hat{b}^\dagger\hat{b} + \omega_{c0}\hat{c}^\dagger\hat{c} + G\hat{c}\hat{b}^\dagger + G^*\hat{c}^\dagger\hat{b}, \qquad (2)$$

where $G = \langle\hat{a}\rangle\, g$ is the effective coupling strength, $|\langle\hat{a}\rangle|^2 \propto P_a$ is the mean photon number of mode a and P_a is the power of the drive laser. This beamsplitter-like Hamiltonian indicates that photons in cavities b and c can be converted to each other coherently without introducing additional noises [26], just like a linear optics device.

It is instructive to introduce a simplified model, as depicted in Fig. 1c, where two resonators loaded by two separate bus waveguides are used to represent the resonant modes b and c separately. The originally independent resonators are coupled together through nonlinear interaction G, which is enabled and controlled by drive laser ω_a. Intuitively the photon flux input from top waveguide can be dropped to the bottom waveguide, or vice versa, analogous to the coupled-microring add-drop filter [27]. Such a device can be schematically illustrated as a four-port block (Fig. 1d), exhibiting two intriguing properties: first, the color of dropped photon changes due to nonlinear wavelength conversion; second, the nonlinear interaction process is non-reciprocal because G vanishes for the probe lights propagating in the opposite direction of the drive laser due to momentum mismatch.

From the device schematic illustrated by Fig. 1c, the most straightforward outcome of the coherent coupling between two resonators is the modified resonance spectrum. When the coupling strength G is comparable or larger than the dissipation rates of the resonators, photons can cycle between the two resonances back and forth coherently and interference can be introduced. The effective frequency and dissipation of the resonance are hence changed due to backactions. We probe such effect us-

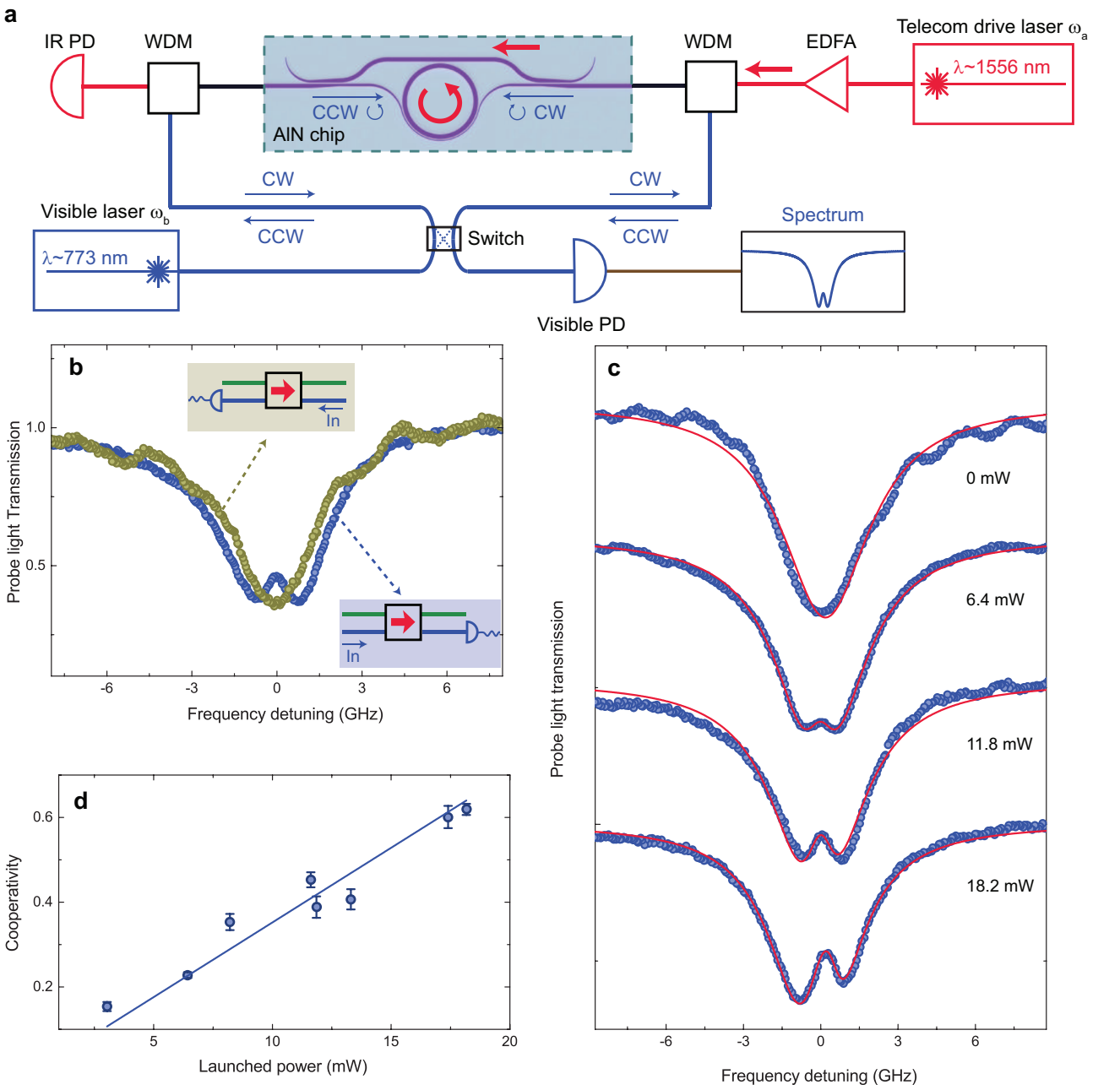

FIG. 2: **Nonlinear optic induced transparency.** **a**, Experimental setup. After amplification with an EDFA, telecom laser ω_a excites mode a in the microring resonator with counter-clockwise (CCW) propagation direction. A visible probe laser ω_b is used to measure the modified transmission spectrum of mode b (centered at ω_{b0}). To verify non-reciprocity, the probe laser's propagation direction is switchable. **b**, Transmission spectra of mode b with both CW and CCW propagation directions. A transparency window is observed if the probe laser propagates in the same direction (CCW) as the drive laser. When the probe laser propagates in the other direction (CW in this case), no transparency window is observed. **c**, NOIT spectra under different powers of the drive laser. The transparency peak's height and width increase with the drive powers, which are labeled in the figure. The red solid lines are fittings with the theoretical transmission formula shown in Eq. 3. The cooperativities can be extracted from the fittings. **d**, Extracted cooperativities at different drive laser powers. A maximum cooperativity of 0.62 is achieved. A linear dependence is observed with an unit power cooperativity to be 0.035 ± 0.001 (1/mW).

ing the experimental setup shown in Fig. 2a. The telecom drive laser (ω_a, near the resonant frequency ω_{a0} of mode a) is amplified with an erbium doped fiber amplifier (EDFA) and excites the counter-clockwise (CCW) propagating mode in the microring, while a visible laser (ω_b) probes the transmission of mode b (centered at ω_{b0}) in either clockwise (CW) or CCW directions, as controlled by an optical switch. Figure 2b plots the spec-

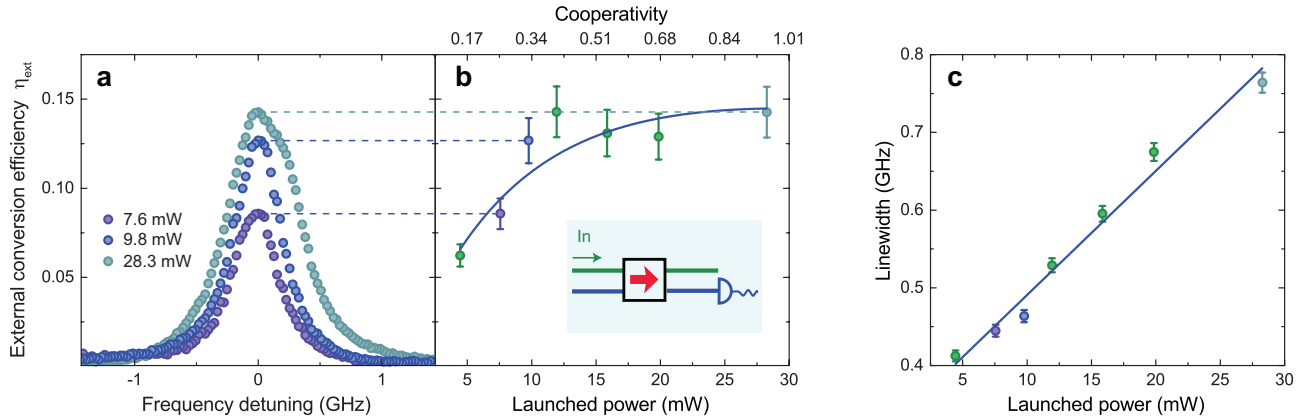

FIG. 3: **Optical frequency conversion from the telecom band to the visible band.** **a**, Frequency conversion spectra with telecom probe laser ω_c tuned across the resonance of mode c under different drive laser powers, which are labeled in the figure. **b**, Maximum external conversion efficiency against different drive power. The error bar comes from the uncertainty of the fiber-to-chip insertion loss. The blue solid line is a fitted curve according to Eq. (5). A unit power cooperativity of $0.034 \pm 0.006\,\mathrm{mW}^{-1}$ is deduced., which is consistent with the values measured in NOIT experiment. Inset, the four-port block model for the frequency conversion process. **c**, The linewidth of the frequency conversion spectra. The error bar comes from the fitting error of each frequency conversion spectrum. A broadened linewidth is observed with the increase of the drive laser power, which results from Purcell effect.

tra of mode b with drive laser ($P_a = 13.3\,\mathrm{mW}$) fixed on the resonance of mode a. A transparency window in the center of the optical resonance is observed when the visible laser propagates in the same direction (CCW) as the drive laser. In contrast, when the probe laser propagates in the counter-propagating direction (CW) of the drive laser, the resonance is of normal Lorentzian shape, similar to the transmission spectrum without parametric pumping (Fig. 2c, top panel). The comparison of the spectra for two propagating directions reveals the nonreciprocal nonlinear effect in the microring, and also unambiguously demonstrates the coherent interaction in a $\chi^{(2)}$ cavity, which manifests as nonlinear optic induced transparency (NOIT).

The observed NOIT is further tested with different powers of the drive laser (Fig. 2c). A clear increase of transparency peak is observed with the increase of launched drive laser power. Following the Hamiltonian (Eq. 2) and considering the linear losses of modes b and c ($\kappa_{x,i}$, $x = b, c$ for two modes and $i = 0, 1$ for intrinsic and external losses), we derive the theoretical formula for the transmission of mode b as

$$T = \left| 1 + \frac{2\kappa_{b,1}}{-i\delta_b - \kappa_b + \frac{|G|^2}{-i\delta_c - \kappa_c}} \right|^2, \qquad (3)$$

where $\kappa_{a(b)} = \kappa_{a(b),0} + \kappa_{a(b),1}$ is total loss rate, $\delta_b = \omega_{b0} - \omega_b$ and $\delta_c = \omega_{c0} - (\omega_b - \omega_a)$ are the angular frequency detunings of mode b and c, respectively. The experimental results are fitted according to Eq. (3) and exhibit valid agreements, as shown by the red solid lines in Fig. 2c. To quantify the strength of coherent nonlinear interaction, the cooperativity $C = \frac{|G|^2}{\kappa_b \kappa_c}$ is extracted from each transmission spectrum and plotted against drive laser power P_a (Fig. 2d). The linear dependence of C over the launched drive power is observed, as expected by theory that $C \propto |G|^2 \propto P_a$. An unit power cooperativity of $C/P_a = 0.035 \pm 0.001\,\mathrm{mW}^{-1}$ is derived and the maximum cooperativity achieved here is 0.62, corresponding to $|G| = 2\pi \times 0.72\,\mathrm{GHz}$. Considering that $\kappa_b = 2\pi \times 1.84\,\mathrm{GHz}$, $\kappa_c = 2\pi \times 0.46\,\mathrm{GHz}$, the system is working inside the NOIT regime ($\kappa_c < |G| < \kappa_b$) [28].

While the NOIT is the hallmark of the coherent interaction, another manifestation of the large C is the high efficiency frequency conversion as the photons drop to different ports (Fig. 1d). The device acts as a beamsplitter for different colors of light and the splitting ratio is controlled by the drive laser. As schematically illustrated in the inset of Fig. 3b, the external conversion efficiency (ratio of output visible photons' number collected by bottom waveguide to the input telecom photons' number in the top waveguide) is measured. By sweeping the telecom input laser frequency ω_c across the resonance of mode c and monitoring the power output near the resonance of mode b (see experimental setup in supplementary section IV), we measure a Lorentzian-like power spectrum (Fig. 3a). The external conversion efficiency reads

$$\eta_{ext} = \frac{\kappa_{b,1}}{\kappa_b}\frac{\kappa_{c,1}}{\kappa_c} \times \frac{4C}{\left|(1 + i\frac{\delta_b}{\kappa_b})(1 + i\frac{\delta_c}{\kappa_c}) + C\right|^2}. \qquad (4)$$

For the cases that $C \lesssim 1$, the maximum external conversion efficiency can be obtained for near-resonance condition that $\delta_c \approx \delta_b \approx 0$

$$\eta_{ext,max} \approx \frac{\kappa_{b,1}}{\kappa_b}\frac{\kappa_{c,1}}{\kappa_c} \times \frac{4C}{|1 + C|^2}. \qquad (5)$$

Figure 3b shows a saturated conversion efficiency against

the launched drive laser power. By fitting the experimental results with Eq. (5), we deduce an unit power cooperativity of $0.034 \pm 0.006\,\mathrm{mW}^{-1}$, which agrees well with the value obtained from NOIT measurement. With the pump power of 28.5 mW, the highest cooperativity we achieve is 0.97 ± 0.17. Accroding to Eq. (5), the saturated external conversion efficiency will be achieved when $C \approx 1$, which is measure to be 0.14 in our experiment. In terms of maximum internal conversion efficiency ($\eta_{int,max} = \frac{4C}{|1+C|^2}$) [25], which ignores the loss due to non-ideal waveguide-cavity coupling ($\frac{\kappa_{b,1}}{\kappa_b}\frac{\kappa_{c,1}}{\kappa_c} < 1$), the conversion efficiency is $0.988 \leq \eta_{int,max} \leq 1$ as deduced from the cooperativity of 0.97 ± 0.17. We further investigate the dependence of the bandwidth of the frequency conversion on P_a, which is shown in Fig. 3c. Owing to a much larger linewidth of mode b compared to that of mode c, the bandwidth of frequency conversion is broadened for large cooperativity C due to the Purcell effect [28]. We get a largest bandwidth of 0.76 GHz with a drive laser power of 28.5 mW.

The cooperativity of the system may be further improved by more sophisticated cavity design to reduce the cavity mode volume while maintaining the high quality factors. Alternatively, by applying high peak power ultrafast driving pulses, the instantaneous C may be improved by 1 or 2 orders of magnitude. The potential applications of the demonstrated non-reciprocal NOIT are all-optical isolators and switches, with the modulation bandwidth exceeding GHz. The external efficiency and bandwidth of the frequency conversion can also be improved, by increasing the external coupling rate of the microring cavity while keeping the cooperativity at 1. For example, if the drive mode photon number increases by 10 times, the maximum achievable external conversion efficiency is about 70% and the bandwidth is about 2 GHz for current experimental parameters. Such devices can be key components for connecting matter qubits at visible wavelength with flying qubits at telecom wavelength, enabling the distributed quantum computation network and quantum communications [29, 30].

Methods

Device fabrication and design parameters. The devices are fabricated using AlN-on-oxide-on-Si chip. After defining the pattern using electronic beam lithography, the waveguide and microring resonators are dry etched using $Cl_2/BCl_3/Ar$ chemistry. We then deposit 2.5 μm thick PECVD oxide on top of the AlN waveguide and anneal the chip in an O_2 atmosphere for 5 h at 950°C. The thickness, width, and radius of AlN microring are 1 μm, 1.12 μm and 30 μm, respectively. The bus waveguide for IR light is 0.8 μm wide with a gap to the microring of 0.6 μm. The wrap around waveguide for visible light is 80 μm long, tapered from 0.175 μm to 0.125 μm, with a gap to the microring of 0.5 μm.

Measurements. Continuous-wave telecom laser (New Focus 6427) is used as the drive laser. After amplification with an EDFA, the drive laser is coupled into the device through an off-chip wavelength division multiplexer (WDM) and a lensed fiber. An on-chip WDM structure is used to guide the telecom drive laser into top bus waveguide and form a counter-clockwise propagating field in the microring resonator. In the NOIT experiment, we use a continuous-wave visible laser (TLB-6712) to probe the transmission spectrum of the visible mode. After coupling into the device through lensed fiber, the visible probe laser is guided to the bottom wrap-around waveguide by the on-chip WDM and forms either clockwise or counter-clockwise propagating light field in the microring resonator. The transmitted visible light is measured by a silicon photoreceiver (New Focus 2001). In frequency conversion measurement, a second telecom laser (New Focus 6428) is used to probe the high Q resonance of mode c. The experimental setup is shown in the supplementary information.

Acknowledgments
The authors thank Liang Jiang for stimulating discussion and Michael Power and Dr. Michael Rooks for assistance in device fabrication. H.X.T. acknowledges support from DARPA and a Packard Fellowship in Science and Engineering. Facilities used for device fabrication are supported by the Yale SEAS cleanroom and the Yale Institute for Nanoscience and Quantum Engineering.

Author contributions
X.G. designed and fabricated the samples, performed the measurements and analyzed the data, C.L.Z. conceived the idea and provided theoretical analysis, H.J. assisted the photonic chip fabrication. H.X.T. supervised the project. All the authors discussed the results and X.G., C.L.Z. and H.X.T. wrote the manuscript.

Competing financial interests
The authors declare no competing financial interests.

[1] Welch, D. F. et al. Large-scale InP photonic integrated circuits: Enabling efficient scaling of optical transport networks. IEEE J. Sel. Top. Quantum Electron. 13, 22–29 (2007).
[2] Khilo, A. et al. Photonic ADC: overcoming the bottleneck of electronic jitter. Opt. Express 20, 4454 (2012).
[3] Shen, Y.R. *The Principles of Nonlinear Optics*. (Wiley, New York, 1984).
[4] Vahala, K. J. Optical microcavities. Nature 424, 839–846 (2003).
[5] Fleischhauer, M. & Marangos, J. P. Electromagnetically induced transparency: Optics in coherent media. Rev.

Mod. Phys. 77, 633–673 (2005).
[6] Moss, D. J., Morandotti, R., Gaeta, A. L. & Lipson, M. New CMOS-compatible platforms based on silicon nitride and Hydex for nonlinear optics. Nature Photon. 7, 597–607 (2013).
[7] Hausmann, B. J. M., Bulu, I., Venkataraman, V., Deotare, P. & Lončar, M. Diamond nonlinear photonics. Nature Photon. 8, 369–374 (2014).
[8] Rakher, M. T., Ma, L., Slattery, O., Tang, X. & Srinivasan, K. Quantum transduction of telecommunications-band single photons from a quantum dot by frequency upconversion. Nature Photon. 4, 786–791 (2010).
[9] Xiong, C. et al. Integrated GaN photonic circuits on silicon (100) for second harmonic generation. Opt. Express 19, 10462–10470 (2011).
[10] Levy, J. S., Foster, M. A., Gaeta, A. L. & Lipson, M. Harmonic generation in silicon nitride ring resonators. Opt. Express 19, 11415–21 (2011).
[11] De Greve, K. et al. Quantum-dot spin–photon entanglement via frequency downconversion to telecom wavelength. Nature 491, 421–425 (2012).
[12] Xiong, C. et al. Aluminum nitride as a new material for chip-scale optomechanics and nonlinear optics. New J. Phys. 14, 095014 (2012).
[13] Kuo, P. S., Bravo-Abad, J. & Solomon, G. S. Second-harmonic generation using 4-quasi-phasematching in a GaAs whispering-gallery-mode microcavity. Nature Commun. 5, 3109 (2014).
[14] Ilchenko, V., Savchenkov, A., Matsko, A. & Maleki, L. Nonlinear Optics and Crystalline Whispering Gallery Mode Cavities. Phys. Rev. Lett. 92, 043903 (2004).
[15] Fürst, J. U. et al. Naturally phase-matched second-harmonic generation in a whispering-gallery-mode resonator. Phys. Rev. Lett. 104, 153901 (2010).
[16] Strekalov, D. V., Kowligy, A. S., Huang, Y.-P. & Kumar, P. Optical sum-frequency generation in a whispering-gallery-mode resonator. New J. Phys. 16, 053025 (2014).
[17] Weis, S. et al. Optomechanically Induced Transparency. Science 330, 1520–1523 (2010).
[18] Safavi-Naeini, A. H. et al. Electromagnetically induced transparency and slow light with optomechanics. Nature 472, 69–73 (2011).
[19] Kim, J., Kuzyk, M. C., Han, K., Wang, H. & Bahl, G. Non-reciprocal Brillouin scattering induced transparency. Nature Phys. 11, 275–280 (2015).
[20] Dong, C.-H. et al. Brillouin-scattering-induced transparency and non-reciprocal light storage. Nature Commun. 6, 6193 (2015).
[21] Jalas, D. et al. What is — and what is not — an optical isolator. Nature Photon. 7, 579–582 (2013).
[22] Tzuang, L. D., Fang, K., Nussenzveig, P., Fan, S. & Lipson, M. Non-reciprocal phase shift induced by an effective magnetic flux for light. Nature Photon. 8, 701–705 (2014).
[23] Peng, B. et al. Parity–time-symmetric whispering-gallery microcavities. Nature Phys. 10, 394–398 (2014).
[24] Dong, C., Fiore, V., Kuzyk, M. C. & Wang, H. Optomechanical Dark Mode. Science 338, 1609–1614 (2012).
[25] Hill, J. T., Safavi-Naeini, A. H., Chan, J. & Painter, O. Coherent optical wavelength conversion via cavity optomechanics. Nature Commun. 3, 1196 (2012).
[26] Huang, J. & Kumar, P. Observation of quantum frequency conversion. Phys. Rev. Lett. 68, 2153–2156 (1992).
[27] Little, B. E., Chu, S. T., Haus, H. a., Foresi, J. & Laine, J. P. Microring resonator channel dropping filters. J. Light. Technol. 15, 998–1005 (1997).
[28] Zhang, X., Zou, C., Jiang, L. & Tang, H. X. Strongly coupled magnons and cavity microwave photons. Phys. Rev. Lett. 113, 15 (2014).
[29] Kimble, H. J. The quantum internet. Nature 453, 1023–1030 (2008).
[30] Raymer, M. G. & Srinivasan, K. Manipulating the color and shape of single photons. Phys. Today 65, 32 (2012).